Mechano-chemical degradation effects on slow crack growth in polyethylene pipes with multiple cracks

Jung-Wook Wee , Alexander Chudnovsky , Suleyman Deveci , Byoung-Ho Choi

PII: S0020-7403(24)00616-7
DOI: https://doi.org/10.1016/j.ijmecsci.2024.109575
Reference: MS 109575

To appear in: *International Journal of Mechanical Sciences*

Received date: 28 February 2024
Revised date: 15 June 2024
Accepted date: 14 July 2024

Please cite this article as: Jung-Wook Wee , Alexander Chudnovsky , Suleyman Deveci , Byoung-Ho Choi , Mechano-chemical degradation effects on slow crack growth in polyethylene pipes with multiple cracks, *International Journal of Mechanical Sciences* (2024), doi: https://doi.org/10.1016/j.ijmecsci.2024.109575

Research highlights

- The mechano-chemical degradation was modeled theoretically based on diffusion-reaction.
- SCG behavior of main crack after multiple initiations in polyethylene pipe was simulated.
- Green's function for crack evolution considering multiple initial cracks was constructed.
- A new lifetime prediction methodology of the crack growth from multiple cracks was proposed and validated.

Revised Manuscript for ***International Journal of Mechanical Sciences***

Mechano-chemical degradation effects on slow crack growth in polyethylene pipes with multiple cracks

*Jung-Wook Wee[a], Alexander Chudnovsky[b], Suleyman Deveci[c] and Byoung-Ho Choi[d]**

[a] School of Mechanical System Engineering, Kumoh National Institute of Technology, 61 Daehak-ro, Gumi, Gyeongbuk, 39177, Republic of Korea

[b] Department of Civil and Materials Engineering, University of Illinois at Chicago, 842 W. Taylor St., Chicago, IL 60607, U.S.A.

[c] Borouge Pte. Ltd., Sheikh Khalifa Energy Complex, Corniche Road, PO Box 6951, Abu Dhabi, UAE

[d] School of Mechanical Engineering, College of Engineering, Korea University, 5-ga Anam-dong, Sungbuk-ku, Seoul, 136-701, Republic of Korea

*Corresponding author: bhchoi@korea.ac.kr (Prof. Byoung-Ho Choi)

Abstract

In a chemically aggressive environment, polyethylene pipes are affected by oxidation-induced brittle fracture as follows: (i) multiple crack initiation through a thin degradation layer, (ii) mechano-chemical discontinuous slow crack growth of a main crack, and (iii) eventual fast fracture. A new analytical model for the second stage is proposed based on a modified crack layer theory. The mechano-chemical degradation of the process-zone medium was modeled theoretically by diffusion-reaction equation. Interactions between cracks immediately follow multiple crack initiations based on Green's function. Also, the parametric study involved several model parameters to provide a physical explanation. Further, this study proposed a theoretical method to estimate the crack lifetime by simulating crack initiation and slow crack growth periods,

providing a new framework for predicting the durability of polyethylene pipes under aggressive chemicals.

Key words

Polyethylene; Slow crack growth; Disinfection; Mechano-chemical degradation; Oxidative environment; Diffusion

1. Introduction

Polyethylene pipes exhibit excellent mechanical properties, processability, flexibility, and ease of installation and maintenance. Currently, polyethylene pipes are commonly used in water, oil, and gas distribution pipelines because of its excellent structural safety after the Kobe earthquake [1, 2]. Although the mechanical strength of polyethylene pipes is lower than that of steel or cast-iron pipes, they have better chemical resistances than that of metallic pipes [3, 4]. In recent decades, the continuously increasing level of polymerization and processing technology and the elaborate control of molecular structures, which includes short-chain branch (SCB) distribution, have enabled rapid advances in the physical and mechanical properties of polyethylene pipes [5-15]. Given these improvements, polyethylene piping is being applied to high-pressure pipelines with large diameters that require a high level of structural integrity [16-22].

Fig. 1 shows that polyethylene pipes undergo ductile failure, accompanied by wall thinning and ballooning, when a relatively high stress is applied to hydrostatic pressure tests [23-25]. At lower stresses, the failure mode changes to brittle fracture with limited plastic deformation. In this brittle fracture, the crack starts near the preexisting defect inside the pipe wall and continues to grow in a quasi-equilibrium manner, referred to as slow crack growth (SCG) [26, 27]. The major failure mode under normal operating stress levels is referred to as brittle fracture [28]. The different slopes of the stress-lifetime plots shown in Fig. 1 indicate that an increase in the mechanical stress for the acceleration tests is restricted to same failure modes as the field failure. Although polyethylene pipes produced according to ISO 4427-1/2 [29, 30] specifications are safe to use with chlorine based disinfectants up to a certain residual chlorine levels (≤0.6 mg/l) and pH ranges (6.5 to 8.5) [31], long term exposure to higher

concentration of disinfectants at relatively higher temperatures may result shorter lifetime of pipes due to severe oxidation in combination with stress, i.e., mechano-chemical degradation (MCD) induced SCG. [32-43]. Lifetime estimation methods for these aggressive chemicals are required because these agents accelerate the brittle fracture of polyethylene pipes compared to that under normal conditions. Therefore, test methods to evaluate the chlorine resistance of polyolefin pipes are standardized in USA, wherein the chlorinated medium is circulated through pipes under hydrostatic loading while maintaining a constant chlorine concentration [44-46]. In addition, NOL Ring Test was developed in France to evaluate resistance of pipes against disinfectants [47]. Although these standard test methods employ elevated temperatures very high level of disinfectants for accelerating failure and requires an extensive testing period of a year.

Small scale tensile coupon tests with periodic characterization were widely used to analyze the oxidative degradation of polyethylene materials for accelerating and easing material testing. Colin et al. [35] characterized the morphological aging behavior of thin polyethylene films in chlorine dioxide, where the decay of the tensile properties and changes in the molecular structure were studied quantitatively. Majewski et al. [48] studied the degradation kinetics of extruded polyethylene films with constant chlorine content. The chain scission-induced decrease in molecular weight, change in crystal structure, and increase in carbonyl index with the immersion period were analyzed. Mikdam et al. [49] assessed and modeled the oxidation behavior of compression-molded polyethylene films with different pH values, wherein the increase in carbonyl band profiles in the thickness direction was simulated and compared with experiments. Bredács et al. [50] investigated the effect of a chlorine dioxide medium on polyethylene thin films with different thicknesses. At a constant concentration of chlorine dioxide, the thinner the specimen, the faster is the degradation of the tensile properties. Yu et al. [51] characterized the antioxidant (AO) depletion kinetics and increased the carbonyl index using thin polyethylene films.

The coupon-based method used to evaluate the deterioration of mechanical properties requires small amounts of material and shortens the test period by increasing the temperature or disinfectant concentration [42, 48]; however, it provides only the chemical degradation behavior of the evaluated specimen geometry under

specific degradation conditions without a load, and mainly evaluates the performance of additive package used in the polymer compound. Moreover, the chemical resistance ranking of different pipe materials obtained in this manner can offer different results at the pipe scale under regular operating conditions (pressure, temperature, disinfectant concentration). The use of thin specimens for expediting material degradation cannot mimic the diffusion of aggressive agents into thick pipe walls with an oxidative reaction, which are referred to as the so-called diffusion-limited oxidation (DLO) behaviors [52-55]. Although many accelerated evaluation methods can be used, predicting the actual lifetime of polyethylene pipes can be challenging without a core model that considers the relationship between the chemical degradation data (via coupon test results), slow crack growth data under load, and combination of chemical degradation and slow crack growth, that is mechano-chemical degradation induced slow crack growth, together with pipe-scale DLO kinetics. For pipe-scale tests, the DLO tendency is different with temperature, wherein the reduced DLO occurs at actual lower temperatures (operating conditions) [56]. Therefore, incorrect results can be obtained using the Arrhenius law if high-temperature test results are used for life prediction under actual low-temperature conditions [57]. Recently, a novel accelerated test method for the second stage based on an ISO standard [58] was proposed, wherein fatigue loading was applied to the cracked round bar (CRB) specimen immersed in chlorinated water [59, 60]. A lifetime divergence caused by uncontrollable asymmetric crack growth can limit the applicability of the results although this approach accomplishes very quick brittle fracture and ranking between materials [61-65]. Further, the effect of oxidation at the crack tip may be underestimated compared to the actual use conditions because exposure duration in fatigue loading can be reduced clearly compared to that in hydrostatic (creep) loading. One method to solve the abovementioned problems is physical modeling, which considers the oxidation behavior and failure stages of the polyethylene pipe.

The MCD induced SCG behavior of polyethylene pipes exposed to oxidative agents is composed of three main stages: (i) multiple crack initiations penetrating the thin degradation layer, (ii) SCG of the main crack through the polymer substance, and (iii) fast fracture (Fig. 2). The last stage occurred within a very short time, and therefore, the remaining two stages governed most of the lifespan. The first stage, i.e., the formation of

a thin degradation layer and simultaneous multiple crack initiation behaviors (Fig. 2b) is successfully modeled and simulated based on an energy analysis performed by the authors [66]. The tendency of multiple crack initiations under severe oxidative conditions was proved, and the simulation results were compared with the experimental results [67]. For the second stage of SCG, the distance between neighboring cracks was relatively close immediately after multiple crack initiations, and therefore, the crack interactions need to be considered. The model needs to capture the well-known discontinuous SCG nature of pipe-grade polyethylene materials [68-74]; the crack layer (CL) model can theoretically simulate the discontinuous SCG behavior of pipe-grade polyethylene in several specimen geometries such as CRB, single-edge notched tension, compact tension, stiff-constant K, and single cracks in pipes [23, 75-81].

In this study, a fundamental model for the second stage of MCD induced SCG, i.e., the discontinuous SCG of the main crack after multiple crack initiations under oxidative degradation was developed. The CL model was modified to consider oxidative degradation caused by the diffused agent near the crack tip and effect of initial multiple cracks. Discontinuous propagation was simulated successfully, and a parametric study of several input parameters was performed to understand the discontinuous MCD induced SCG behavior. A new lifetime estimation method based on multiple crack initiations and SCG periods is proposed based on the developed model.

2. Failure behavior of polyethylene pipes under an oxidative environment

High concentration of free chlorine above suggested dosing levels accelerates the consumption of AO in polymer compound when polyethylene pipes are used to transfer water containing disinfectants [3, 67, 82, 83]. The oxidative agents diffuse through the inner surface via oxidative reactions and consumed by a chemical reaction; therefore, the diffusion into the sink should be considered. The polymer medium undergoes oxidative degradation after AO depletion because pipe-grade polyethylene materials contain AO packages [51]. The diffusion of AO into the fluid flowing inside the pipe, i.e., the washing out of AO is an additional factor that accelerates AO consumption [3, 84]. The thin degradation layer is formed at the inner surface with a thickness of 150~200 μm because of the oxidation of the polymer medium (Fig. 2b) [32]. Oxidation is

manifested as a chain scission, which leads to embrittlement and densification. The thin degradation layer shrinks because of oxidation, whereas the undegraded polymer medium remains unchanged. Such behavior results in additional tangential stress on the thin degradation layer and oxidation-induced toughness reduction in this thin region [33]. Cracking eventually occurs after a certain operating time; wherein multiple radial cracks form simultaneously throughout the thin layer (Fig. 2c). Multiple cracks are widely reported in the literature [32, 34, 85, 86]. In addition, a theoretical model of this multiple-crack initiation behavior has been proposed based on energy analysis [66]. Because the size of the multiple initial cracks of 150~200 μm are quite large than the spherulite of the polyethylene (~5 μm) [87], the crack initiation models were conducted based on the assumption of the homogeneous medium.

After crack initiation, the main crack grows and penetrates the pipe wall in a quasi-equilibrium manner, as indicated in Fig. 2d. For the pipe-grade polyethylene, a wedge-shaped damage zone (process zone, PZ) forms in front of the crack tip [76, 88]. Experimental observations revealed that PZ is composed of cold-drawn fibrils; i.e., the PZ evolution acts as an energy barrier against the crack growth. The crack arrest period representing the amount of time required for the PZ medium to degrade sufficiently exists for a discontinuous SCG. The PZ medium decays through mechanical creep and an oxidative reaction by a diffused agent when the pressurized polyethylene pipe transports the oxidative fluid, thereby causing mechano-chemical degradation (Fig. 2f) [33, 34, 89, 90]. Instability occurs if the quasi-equilibrium growth of the PZ and main crack reaches a certain length, and the fast fracture results in a final leakage or burst fracture (Fig. 2e).

3. Modeling

3.1 Green's function for a single crack after multiple crack initiations

The constitutive equations for the crack layer growth are described in Appendix A. The determination of the K_{tot} and δ_{tot} in the constitutive equations, as derived in Eq. (A.2), is explained in this section. Because K_{tot} and δ_{tot} represent the SIF at the PZ tip and COD at the crack tip for the PZ-cutoff elastic solid, respectively, enabling the effect of

internal pressure (p_i) and drawing stress (σ_{dr}) to be examined independently and superimposed (Fig. A.1). The SIF caused by p_i (denoted as K_∞) was determined by finite element analysis (FEA) in the configuration shown in Figs. 3a and 3b. The 1/2" diameter pipe with a standard dimension ratio of 9 was considered. The number of initial cracks is denoted by N, with the same initial crack length a_i. Among the multiple initial cracks, the length of the main crack is denoted by a. In this study, the notation of a indicates the crack length of PZ-cutoff elastic solid for the formulation of the Green's function. A half model along the main crack plane is used as shown in Fig. 3c, and the mid-side node parameter is applied to achieve crack-tip singularity (Fig. 3d). The pressure on the inner surface of the pipe is exerted by p_i (Fig. 3c); the deformation at N = 1200 is shown in Fig. 3e. Detailed views of the deformation of the nearby and main cracks are presented in Figs. 3f and 3g, respectively.

For single crack initiation and growth (N = 1), a_i equals zero, and the normalized K_∞ against the normalized single crack length (a/W) with a range from 0.01–0.8 is obtained as shown in Fig. 4a and listed in Table 1. The normalized initial crack length $\bar{a}_i = a_i/W$ value in the range from 0.01–0.2 was considered for multiple crack initiation because the crack initiation size is considerably shorter than the pipe thickness. Further, N was considered by 4, 36, 360, 1000, 1200, 1500, and 2000. Immediately after multiple crack initiations, a equals a_i, and the main crack propagates in a quasi-equilibrium manner until a = W, where W represents the pipe wall thickness. Therefore, a FEA was performed for the normalized main crack length, $\bar{a}=(a-a_i)/(W-a_i)$ from 0–0.8. For multiple crack initiation, crack interaction differentiates the normalized K_∞ despite the same main crack length a. As shown in Fig. 4b for a_i/W = 0.01, the distance between the adjacent initial crack decreases with an increase in N, and therefore, the N = 2000 case has the lowest K_∞ when a and a_i are similar. The effect of adjacent initial cracks becomes significant with an increase in a_i (Figs. 4c and 4d for $\bar{a}_i$ = 0.1 and 0.2, respectively). The larger the initial crack clusters distributed vertically with a closer distance, the greater is the crack shielding effect at the early stage of the main crack growth. The data for normalized K_∞ with the number of cracks N and normalized geometric parameters $\bar{a}_i$ and $\bar{a}$ are listed in Table 2. During the simulation, the interpolation method was used to determine K_∞ based on Tables 1 and 2.

The SIF caused by the constant stress distribution along the PZ ($l_{CR} \le x \le L$ in Fig. A.1)

must be determined in any combination of l_{CR} and L for computing the SIF attributed to σ_{dr} (denoted by K_{dr}). An easy method for constructing SIF Green's function (G^{SIF}), which is the so-called weight function, for the considered cracked geometry [26]. In this study, the G^{SIF} for various multiple-crack configuration parameters was built using the FEA method. Figs. 5a and 5b shows that the SIF caused by the unit dipole force on the main crack surface at x can be obtained using the FEA method, where an example of the deformation behavior is shown in Fig. 5c. The crack tip model shown in Fig. 3d is used. Further, Fig. 6 exhibits the normalized G^{SIF} against the normalized x, $\bar{x} = (x - a_i)/(a - a_i)$, for the various main crack lengths in the N = 4 and 1200 case. The FEA results represented by the symbols are fitted using [91],

$$G^{SIF}(N, a_i, a; x) = \frac{1}{\sqrt{2\pi a}}[c_1(1-\bar{x})^{-0.5} + c_2(1-\bar{x})^{0.5} + c_3(1-\bar{x})^{1.5}], \quad (1)$$

where coefficients c_1–c_3 are functions of N, $\bar{a}_i$, and $\bar{a}$, respectively. Fig. 6 shows curves fitted using Eq. (1) agrees well with the FEA results, and the lowest R-squared value for all cases is 0.9893, which indicates the high accuracy of Eq. (1). For single crack initiation and growth (N = 1), G^{SIF} is a function of $\bar{a}$ and $\bar{x}$, and coefficients c_1–c_3 depend on $\bar{a}$. The fitted c_1–c_3 values for N = 1 are listed in Table 3. Further, the fitted values of c_1, c_2, and c_3 for multiple crack initiations (N = 4–2000) are listed in Tables 4, 5, and 6. During the simulation, c_1–c_3 were estimated using the interpolation method, and G^{SIF} was determined using Eq. (1). Then, the K_{dr} can be computed easily by the following integration of G^{SIF} along the PZ boundary, $l_{CR} \le x \le L$,

$$K_{dr} = -\sigma_{dr}\int_{l_{CR}}^{L} G^{SIF}(N, a_i, a; x)dx, \quad (2)$$

where the negative signs in Eq. (2) arising from σ_{dr} tends to close the main crack. Further, the K_{tot} in Eq. (A.2) can be computed by the superposition of K_∞ and K_{dr}, i.e., $K_{tot} = K_\infty + K_{dr}$ [76].

The COD attributed to p_i, denoted by δ_∞ near the PZ tip, is estimated by [92]

$$\delta_{\infty}(x) = \frac{8K_{\infty}}{E'}\left[\frac{(L-x)}{2\pi}\right]^{0.5}, \quad (3)$$

where E' represents the elastic modulus (plane strain) of the PZ-cutoff elastic medium. The COD caused by σ_{dr}, denoted by δ_{dr}, is computed based on the COD Green's function (G^{COD}), which indicates the COD profiles caused by the unit dipole force shown in Fig. 5c. G^{COD} can be expressed by G^{SIF} based on Castigliano's theorem [81, 93].

$$G^{COD}(N, a_i, a; x_0, x_1) = \frac{2}{E'}\int_{\max(x_1, x_0)}^{a} G^{SIF}(N, a_i, \xi; x_0) \cdot G^{SIF}(N, a_i, \xi; x_1)\, d\xi. \quad (4)$$

Similar to K_{dr}, δ_{dr} can be written by

$$\delta_{dr}(x) = -\sigma_{dr}\int_{l_{CR}}^{L} G^{COD}(N, a_i, a; x_0, x) dx_0. \quad (5)$$

Consequently, $\delta_{tot}|_{x=l_{CR}}$ in Eq. (A.2) is determined by $\delta_{tot} = \delta_{\infty} + \delta_{dr}$ at $x = l_{CR}$ [76].

3.2 Diffusion of the oxidative agent on the process zone with chemical reactions

During the SCG process, the oxidant at the crack tip diffuses into the PZ medium when in contact with the oxidative fluid, which is composed of highly drawn fibrils (Fig. 2f). The concentration of the oxidant in the PZ according to coordinates x and time t is defined as $C(x, t)$. In addition, the diffused oxidant can be consumed by an oxidative reaction with the AO, and therefore, the constitutive equation of diffusion with the chemical reaction can be written as [66]

$$\frac{\partial C}{\partial t} = D\frac{\partial^2 C}{\partial x^2} - R(C), \quad (6)$$

where $R(C)$ represents the removal rate of the oxidant and is a function of current concentration C. In this study, it is assumed that the oxidant removal rate was proportional to the local coefficient $C(x, t)$, and $R(C) = k_R C$ was substituted; the k_R indicates the reaction rate constant [66]. The diffusion medium is assumed to be semi-

infinite along x; the convection boundary condition at the crack tip (x = 0) is considered [89, 90, 94]. The boundary conditions (BCs) were

$$C(\infty, t) = 0 \quad \text{and} \quad k[C_\infty - C(0,t)] = -D\frac{\partial C}{\partial x}\Big|_{x=0}, \tag{7}$$

where k and D denote the mass-transfer and diffusion coefficients, respectively. C_∞ represents the oxidant concentration in the environment (see Fig. 2). The initial zero-concentration condition is employed using the following condition,

$$C(x, 0) = 0. \tag{8}$$

The equations (10–12) can be solved analytically, as explained in detail in Appendix A. The solution of the concentration is given by

$$\frac{C(x,\,t)}{C_\infty} = \frac{ke^{-k_R t}}{D}\left[\frac{1}{2}e^{k_R t}\left\{\frac{\sqrt{D}}{\frac{k}{\sqrt{D}}+\sqrt{k_R}}e^{-x\sqrt{\frac{k_R}{D}}}\,erfc\left(\frac{x}{2\sqrt{Dt}}-\sqrt{k_R t}\right)\right.\right.$$
$$\left.\left.+\frac{\sqrt{D}}{\frac{k}{\sqrt{D}}-\sqrt{k_R}}e^{x\sqrt{\frac{k_R}{D}}}\,erfc\left(\frac{x}{2\sqrt{Dt}}+\sqrt{k_R t}\right)\right\}\right.$$
$$\left.-\frac{k}{\frac{k^2}{D}-k_R}e^{\left(\frac{k}{D}x+\frac{k^2}{D}t\right)}\,erfc\left(\frac{x}{2\sqrt{Dt}}+\frac{k\sqrt{t}}{\sqrt{D}}\right)\right]. \tag{9}$$

The diffusion behavior was visualized to validate the derived analytical solution. Concentration profiles against the normalized x and t with various k_R are presented in Figs. 7a, 7b, and 7c, for the k_R = 2E−12, 1E−11, and 5E−11 s^{-1}, respectively. An increase in k_R leads to an accelerated consumption of the diffused oxidant, reducing the overall concentration distribution. Fig. 7d shows the normalized concentration at x = 0. The $C(0, t)/C_\infty$ is plotted against the normalized time (k^2t/D), which demonstrates that the increased consumption rate results in a limited oxidant concentration growth at the crack tip (x = 0). Concentration profiles in the PZ medium at different diffusion times are shown in Fig. 7e. The concentration profile increased with time through the diffusion of

the oxidant from the crack tip. Therefore, the diffusion behavior of the chemical reaction along the PZ medium was solved properly, thereby revealing the appropriate behavior of the analytical solution.

3.3 Mechano-chemical degradation of process zone

The oxidant diffused into the PZ and was consumed by a chemical reaction with AO. Once the AO is completely consumed by the chemical reaction with oxidant, the polymer chains become unprotected, leading to chain scission and a decrease in toughness within the PZ medium. An additional decay of the PZ medium was manifested by the faster decrease of 2γ during the crack arrest period. The polymer chain scission the PZ medium attributed to the oxidative reaction can be explained based on the analytically solved diffusion behavior. If the chemical degradation (for polymer chains) parameter within the PZ medium as $\omega(x, t)$ is defined, the rate of degradation parameter through the oxidation would be a monotonic function with $R(C)$ and can be expressed as

$$\frac{\partial \omega}{\partial t} = f_{\omega}\big(R(C)\big). \tag{10}$$

It is worth noting that the ω is related to the degradation of polymer chains, not to the AO depletion. With the assumption that the monotonic function f_{ω} is first order with $R(C)$, the rate of the degradation parameter is given by $k_{\omega}R(C)$, where k_{ω} represents a proportional constant. Considering that $R(C) = k_R C$ and t_{OIT} (oxidation induction time, OIT, for the depletion of anti-oxidants, AO, at the operating condition), the degradation parameter $\omega(x, t)$ can be rewritten by [66]

$$\omega(x,t) = k_{\omega}k_R \int_0^t C(x, t - t_{OIT})dt. \tag{11}$$

The degradation parameter ω has a range from 0 to 1, where ω for the unaged material is 0, and ω equals to 1 for the fully degraded material [32, 34]. The example behavior of the degradation parameter ω at the crack tip is revealed in Fig. 7f. The chemical degradation does not occur before t_{OIT}, and $\omega = 0$ for this period ($0 \le t \le t_{OIT}$). After t_{OIT}, ω starts to grow up to 1 following Eq. (11), and then, it remains as a fully degraded state ($\omega = 1$).

The decay of 2γ caused by the oxidation is expressed by the degradation parameter ω, followed by

$$2\gamma = 2\gamma_0(1-\omega)^{2.4}, \quad (12)$$

where the exponent 2.4 is adopted from the experimental work [32]. The total mechanochemical decay of the PZ medium can be expressed by superposition because PZ under an external load undergoes mechanical degradation [33, 90].

$$2\gamma = 2\gamma_0\left\{(1-\omega)^{2.4} - \left(1 - \frac{1}{1+\frac{t_i}{t^*}}\right)\right\}, \quad (13)$$

where the first term in the curly brackets denotes chemical degradation through oxidation, whereas the mechanical degradation caused by the creep is manifested in the second term. No oxidative reaction occurs before t_{OIT}, and therefore, the mechanical decay governs PZ degradation. However, 2γ is dramatically decreased by the chemical degradation after t_{OIT}. After t_{OIT}, chemical degradation dominates the PZ decay mechanism (Fig. 7g).

During the pipe operation, the chlorine species near the inner surface accelerates the oxidation, causing the AO to be consumed preferentially, before the degradation of the PE substance. The initially evenly distributed AO would migrate to the degrading region as a result of this AO concentration gradient. Additionally, after the crack initiation, the AO consumption within the PZ lowers the AO concentration through the pipe wall. Thus, the initial AO concentration of newly formed PZ should decrease with the exposure period. Furthermore, the AO washing out into the transporting fluid can also reduce continuously the amount of the AO content.

Such physical phenomena could be reflected in the model by decreasing the t_{OIT} of the PE pipe with the operating time. Viebke and Gedde [95] measured the average OIT of the wall cross-section of polyethylene pipes containing hot water under hydrostatic pressure and found that the average OIT along the pipe wall thickness decreased linearly with the square root of the elapsed time, $t^{0.5}$. Therefore, the OIT reduction behavior with the total elapsed time t could be written by

$$t_{OIT}(t) = t_{OIT}(0) - k_{OIT}t^{0.5}, \quad (14)$$

where $t_{OIT}(t)$ and $t_{OIT}(0)$ denote the present and initial OIT, respectively. The k_{OIT} represents a constant reduction coefficient related to the OIT. CL growth simulations were performed using the above set of auxiliary models for the SC crack growth after multiple crack initiations. Based on the abovementioned constitutive equations, the CL growth algorithm is described in Fig. 8.

4. Applications

4.1 Parametric study

The sensitivity of several physical parameters was assessed to validate the applicability of the developed model for the SCG in the SCC. The 1/2" polyethylene pipe conveying the oxidative fluid under the constant internal pressure (p_i) at the elevated temperature (95°C) was considered [66, 67]. The effect of the number of initial cracks (N) was investigated, and the initial crack lengths (a_i) (0.2 mm with N = 1 (single crack initiation), 4, 36, 360, 1200, and 2000 (multiple crack initiations)) were examined. The other physical parameters are listed in Table 7. Fig. 9a shows that the discontinuous CL growth behavior is achieved successfully, where an increase in N reduced the crack jump lengths and increased the crack arrest period, thereby extending the SCG duration. The SIF of the main crack during the initial SCG period declined clearly with increasing N because of the crack shielding effect from the neighboring cracks. Therefore, the initial SIF is reduced when N is increased even under the same p_i and a_i, which results in delayed SCG behavior. The decrease in t_{OIT} during the total time following Eq. (14) is shown in Fig. 8b. Further, t_{OIT} decreased during the crack initiation period (t_{CI}), and subsequently, t_{OIT} decreased further during the SCG duration (t_{SCG}). The $\log(da/dt)$ vs. $\log(K_I)$ plots are presented in Fig. 8c. The increase in N lowers the initial SIF, whereas the overall plots shift upward and the slope decrease with N. The normalized SFE, $2\gamma/J_I^{CR}$, with the elapsed time is shown in Fig. 8d. At the initial crack arrest period, 2γ is considerably larger than J_I^{CR}, and therefore, X^{CR} in Eq. (A.2) was negative. 2γ is decreased by Eq. (A.3), and the crack jumps to the PZ tip when 2γ reaches J_I^{CR} (see horizontal dotted line for $J_I^{CR} = 2\gamma$ in Fig. 8e). When N = 1 or 36, the J_I^{CR} has larger values, and $2\gamma/J_I^{CR}$

can become a unit value before t_{OIT}. The 2γ of the PZ medium decays by the mechanical degradation only in such cases; however, when N = 1200, a considerably lower value of J_I^{CR} occurred initially, and the crack-arrest periods extended beyond the current t_{OIT}. Therefore, the chemical degradation appears and the 2γ is reduced dramatically by mechano-chemical degradation following Eq. (13) (shown in Fig. 8e). This behavior is manifested in the higher crack growth rate at the same SIF in Fig. 8c because of chemical degradation; for example, N = 360, 1200, and 2000.

The effect of p_i at N = 1200 was investigated, and p_i was changed by 0.5, 0.6, 0.7, and 0.8 MPa, whereas other parameters are the same as in Table 7. Mechanical degradation cases without chemical degradation were simulated and compared to examine the effects of chemical degradation. Figs. 9a and 9b show the CL growth patterns of different p_i under mechanochemical degradation and mechanical degradation only, respectively. An increase in p_i clearly accelerated CL growth because of the increase in driving terms in Eq. (A.2). Fig. 9c shows that the curves for the mechanical degradation cases collapse into one representative curve regardless of the p_i if the crack growth behaviors are reduced to the da/dt–K_I plots; this is the same with the previous results [23, 80, 96]. However, the SCG rate curves differed with applied p_i in the mechanochemical degradation cases. The higher the p_i, the lower is the SCG rate at the same SIF. The initial SIF decreased with a decrease in p_i, and a longer elapsed time was required for the same SIF. Therefore, an increased SCG rate can be observed because t_{OIT} decreases further at the same SIF. This behavior can be observed in Fig. 9d, where the ratio of the SCG rate for mechanochemical degradation ($(da/dt)_{mc}$) to that for mechanical degradation, $(da/dt)_m$, is depicted. The SCG rate converges to the mechanical degradation case because the driving term in Eq. (A.2) is sufficiently high compared to 2γ at the high level of SIF, regardless of the p_i, which is similar to the literatures [33, 89, 90]. The overall $2\gamma/J_I^{CR}$ plots and the enlarged view at the initial crack are shown in Figs. 9e and 9f, respectively.

The effects of the reaction rate coefficient k_R are illustrated in Fig. 10. k_R physically reflects the resistance to the oxidative degradation of the polyethylene material itself after AO depletion because k_R is influenced after t_{OIT}. The increase in k_R suggests a faster chemical reaction as well as rapid consumption of the diffused oxidant. In addition, the faster the oxidant consumption, the quicker is the diffusion of environmental oxidants

into the PZ medium. Therefore, the SCG duration is reduced dramatically with an increase in k_R (Fig. 10a). Variations in t_{OIT} during the SCG period are shown in Fig. 10b. k_R =1E−11 s^{-1} and the rapid chemical decay results in the shortened crack arrest periods, and therefore, the SCG rate (da/dt) is markedly increased compared to the lower k_R cases or the mechanical degradation case as shown in Fig. 10c and 10d. The effect of chemical degradation is insignificant if k_R has an extremely low value, i.e., k_R = 1E−15 s^{-1}, which leads to a similar SCG rate with mechanical degradation caused by crack grows. Further, at k_R = 1E−11 s^{-1}, the crack arrest period is approximately identical to the same current t_{OIT} because of the rapid chemical degradation; therefore, $(da/dt)_{mc}$ is significantly higher than the $(da/dt)_m$ for major part of the SCG period. The mechanochemical decay of 2γ for a different k_R is shown in Figs. 10e and 10f.

The performance of the AO package in delaying an immediate attack on the polymer substance can be expressed by Eq. (14). Fig. 11 shows SCG behavior with different $t_{OIT}(0)$ values, i.e., $t_{OIT}(0)$ = 2000, 3000, and 4000 h. Fig. 11a shows that the SCG period was significantly extended with $t_{OIT}(0)$ because of the increased overall $t_{OIT}(t)$ during the SCG (see Fig. 11b). Figs. 11c and 11d show that, with a decreasing $t_{OIT}(0)$, the SCG rate appears to increase by moving forward the start of the chemical degradation, as shown in Fig. 11e and in the enlarged view (Fig. 11f), respectively. Consequently, it was demonstrated that the proposed model exhibited physically appropriate behavior when several important parameters were varied.

4.2 Total lifetime estimation methodology

The crack initiation stage should be considered to estimate the total lifetime of polyethylene pipes conveying oxidative fluids. In the SCC process, crack initiation occurs on the thin degradation layer on the inner surface of the pipe caused by severe DLO kinetics. The combination of the additional tangential stress within the degradation layer resulting from oxidation-induced densification and the reduced toughness in this region causes sudden crack initiation through this degraded layer [32]. Experimental studies showed that multiple initial cracks are produced when the intensive oxidative degradation is accompanied [34, 85]. A fundamental model for multiple crack initiation behavior was suggested by the authors, and the experimental results were simulated

accurately [66, 67]. At the same operating conditions, i.e., 1/2" polyethylene pipe at 95 °C in chlorine environments, the simulation results for the crack initiation are summarized in Table 8. Multiple cracks with an average number of N = 1200 were produced because of the significant influence of oxidation at low p_i, whereas single cracking (N = 1) occurred at high p_i, which indicates a normal brittle fracture with a less oxidation effect. Crack initiation time (t_{CI}) and length of the initial crack (a_i) were estimated in a previous study [66]. After these initial cracks, the SCG behavior of the main crack is simulated using the present model according to Table 8. Input parameters except N, a_i, and t_{CI} are the same as those in Table 7. Cracks tended to be generated in multiple ways with a decrease in p_i, and the SCG period was obviously extended, as shown in Fig. 12a. The reduction behavior of t_{OIT} with elapsed time is shown in Fig. 12b. t_{OIT} in the initial SCG stage has different values because t_{CI} is different from p_i. At a low level of p_i, the SCG rate (da/dt) at the same K_I is increased because the t_{OIT} is sufficiently decreased by the extended elapsed time, which indicates the increased oxidative degradation effect on the 2γ decay (Fig. 12c). The SCG duration (t_{SCG}) and N with respect to p_i are shown in Fig. 12d. Based on the proposed model, the total lifetime (t_f) of a polyethylene pipe can be expressed as

$$t_f = t_{CI} + t_{SCG}. \quad (15)$$

The p_i–t_f plots can be established as shown in Fig. 12e. The square and circular symbols denote t_{CI} and t_f, respectively. On a log–log scale, the chemical knee, which has been widely reported in literature, can be found in this simulation [24, 61, 97]. Above the chemical knee, a common brittle fracture arises from single crack initiation and growth, which is related to the mechanically dominated region. At a lower p_i, the oxidation-induced multiple crack initiation as well as the mechano-chemical SCG of the main crack cause a stiffer slope in the p_i –t_f plot, indicating a lower dependency of the applied stress level on the final lifetime. The total SCC lifetime of polyethylene pipes can be estimated theoretically through the fundamental models of crack initiation and growth in contact with an aggressive chemical.

5. Conclusions

When transporting oxidative fluids, polymer pipes generate a thin deterioration layer caused by oxidative degradation on the inner surface, initiating multiple cracks passing through the deterioration layer. The PZ in front of the main crack tip undergoes mechanochemical deterioration, and the discontinuous SCG of the main crack causes final failure. The mechanochemical discontinuous SCG behavior of the main crack after multiple crack initiations on a polyethylene pipe was simulated theoretically in this study.

Green's function for the main crack was constructed considering multiple initial cracks, and it was applied to the CL evolution model. An analytical solution for the diffusion of the oxidative agent into the PZ was derived via reaction-induced consumption. The mechanochemical degradation behavior in the PZ medium was modeled based on this solution. Further, AO depletion was also considered during the operating period. A sensitivity study on the several input parameters, e.g., number of initial cracks N, internal pressure p_i, reaction rate coefficient k_R, and initial oxidation induction time $t_{OIT}(0)$, was performed to validate the developed model. Further, discontinuous SCG, which is observed in pipe-grade polyethylene, was also observed. The adequacy of the proposed model was evaluated through a sensitivity study of several parameters, and changes in the mechanochemical discontinuous SCG behavior with the input parameters were explained physically.

A new lifetime prediction methodology using multiple crack initiation and crack growth models was proposed based on the proposed model. Lifetime estimation with internal pressure (p_i) was performed successfully to capture the chemical knee point, which classified the failure mechanism into mechanical- (single crack initiation) and chemical-dominated regions (multiple crack initiation).

CRediT authorship contribution statement

Jung-Wook Wee: Conceptualization, Methodology, Validation, Formal analysis, Investigation, Data curation, Writing – Original draft, and Visualization; **Alexander Chudnovsky:** Conceptualization, Resources, Methodology; **Suleyman Deveci**:

Conceptualization, Resources, Writing – Review and editing; **Byoung-Ho Choi:** Methodology, Writing – Review and editing, Investigation, Supervision, Project administration.

Declaration of Competing Interest

The authors declare that they have no competing financial interests or personal relationships that may have influenced the work reported in this study.

Acknowledgements

This work was supported by National Research Foundation of Korea grants funded by the Korean government (MSIT) (No. RS-2024-00347187) and was supported by the Ministry of Trade, Industry and Energy (MOTIE), Korea Institute for Advancement of Technology (KIAT) through the Virtual Engineering Platform Program (P0022334). This study was also supported by Borouge Pte. Ltd.

Appendix A. Constitutive equations for crack layer growth model

As shown in Fig. 3a, the main crack and surrounding PZ propagates in a quasi-equilibrium manner after multiple crack initiations with length a_i and number N. Let us assume that the evolution of the CL system of the main crack is defined by determining the CL configuration parameters for the main crack, i.e., the crack length (l_{CR}) and CL length (L), with elapsed time. The remaining initial cracks did not grow over time, except for the main crack. The thermodynamic force for the growth of l_{CR} and L can be written as the variation in the total Gibbs potential energy (G_{tot}) with the CL configuration parameters [26, 76]:

$$X^{CR} = -\left.\frac{\partial G_{tot}}{\partial l_{CR}}\right|_{L} \quad \text{and} \quad X^{PZ} = -\left.\frac{\partial G_{tot}}{\partial L}\right|_{l_{CR}}, \tag{A.1}$$

where X^{CR} and X^{PZ} represent the thermodynamic forces for crack and PZ growth, respectively. A narrow PZ shape with a clear boundary and undamaged medium allows

the decomposition of the entire CL system into the PZ-cutoff elastic medium for polyethylene (Fig. 3b) and the PZ medium (Fig. 3c). Traction along the hypothetical boundary is assumed to be consistent with the drawing stress (σ_{dr}) of the polyethylene material. The additional assumption that the PZ medium is composed of fully drawn fibrils up to their natural draw ratio (λ) enables rewriting X^{CR} and X^{PZ} as computable terms [76].

$$X^{CR} = J_I^{CR} - 2\gamma \quad \text{and} \quad X^{PZ} = \frac{K_{tot}^2}{E'} - \frac{\gamma^{tr}}{\lambda - 1}\delta_{tot}|_{x=l_{CR}}, \tag{A.2}$$

where J_I^{CR} represents the energy release rate at the crack tip, whereas 2γ denotes the specific fracture energy (SFE) at the crack tip. Further, K_{tot} in X^{PZ} represents the mode-I stress intensity factor (SIF) at the PZ tip of the PZ-cutoff elastic medium caused by a combination of the internal pressure p_i and σ_{dr}, as shown in Fig. 3b. The PZ medium was created by drawing the original material with width $w_0(x)$ into $w(x)$ (Fig. 3d). The difference between $w_0(x)$ and $w(x)$ can be obtained by the total crack opening displacement (COD, δ_{tot}) attributed to p_i and σ_{dr}. E' represents the plane strain elastic modulus and γ^{tr} represents the energy density for the transformation from the original to the PZ medium. A detailed explanation of the CL growth model under mechanical loading can be found in the literature [26, 78, 81].

According to the discontinuous SCG behavior, the newly formed PZ medium shows a higher SFE (2γ) than the current J_I^{CR}, which indicates a negative X^{CR} and a crack arrest period. The 2γ of the PZ medium is degraded by mechanical creep during the crack arrest period under only mechanical loading. The mechanical degradation behavior can be expressed by [98],

$$2\gamma = 2\gamma_0 \frac{1}{1 + \frac{t_i}{t^*}}, \tag{A.3}$$

where $2\gamma_0$, t_i, and t^* represent the initial SFE of the undegraded polyethylene, elapsed time after the transformation to the PZ, and characteristic time of mechanical degradation, respectively. If 2γ is sufficiently decreased for $X^{CR}>0$, the crack penetrates into the PZ medium and PZ starts to grow simultaneously until $X^{PZ}\leq 0$. The repeated crack arrest growth behavior results in discontinuous and stepwise SCG growth

patterns in polyethylene [79]. For the SCC environment, the oxidation-induced chemical degradation may strongly promote the decay of 2γ [33].

When X^{CR} and X^{PZ} are used to determine the current CL configuration using the above set of equations, the growth rate of the CL configuration parameters l_{CR} and L can be explained by [81, 99],

$$\dot{l}_{CR} = k_{CR}X^{CR} \quad \text{and} \quad \dot{L} = k_{PZ}X^{PZ}, \tag{A.4}$$

where k_{CR} and k_{PZ} represent the constants related to the crack and PZ evolution, respectively. The discontinuous CL growth patterns of polyethylene specimens are simulated successfully using the CL model accompanied by a time-marching loop algorithm [23, 76, 77, 79]. The abovementioned CL growth model can be applied to all crack-containing geometries, provided X^{CR} and X^{PZ} are properly determined for the current CL configuration. K_{tot} and δ_{tot} in X^{PZ} vary with the current l_{CR} and L, in addition to the initial crack length (a_i) and number of initial cracks (N) caused by crack interactions. Therefore, it is useful to formulate Green's functions for K_{tot} and δ_{tot} and various other geometry parameters. Fig. 3a shows the determining procedure of K_{tot} and δ_{tot} based on Green's function for the main crack with multiple initial cracks.

Appendix B. Analytical solution of diffusion with a reaction

The governing equation of the diffusion with the reaction for $C(x, t)$ is given by the following partial differential equation (PDE) for variables x and t.

$$\frac{\partial C}{\partial t} = D\frac{\partial^2 C}{\partial x^2} - k_R C, \tag{B.1}$$

where the BC and initial conditions (IC) are the same as those in Eqs. (11) and (12). Let the Laplace transform of the $C(x, t)$ regarding the positive real $t \geq 0$ is given by

$$\mathcal{L}\{C(x,t)\} = \int_0^\infty C(x,t)e^{-st}dt = U(x,s). \tag{B.2}$$

Then, the Laplace transform of Eq. (B.1) becomes

$$sU(x,\ s) - C(x,\ 0) = D\frac{\partial^2 U}{\partial x^2} - k_R U(x,s), \tag{B.3}$$

where the second term becomes zero by the IC. Equation (B.3) can be rewritten as the following ordinary differential equation (ODE) for variable x as

$$\frac{\partial^2 U}{\partial x^2} = \left(\frac{k_R + s}{D}\right) U(x,s). \tag{B.4}$$

The general solution of the above ODE is

$$U(x,s) = c_1 e^{-\sqrt{\frac{k_R+s}{D}}x} + c_2 e^{\sqrt{\frac{k_R+s}{D}}x}, \tag{B.5}$$

where c_2 should be zero because of the first BC, i.e., $C(\infty, t) = 0$. The coefficient c_1 can be found using the second BC. The Laplace transform of the second BC is given by

$$\frac{C_\infty}{s} - U(0,s) = -\frac{D}{k}\frac{\partial U}{\partial x}\Big|_{x=0}. \tag{B.6}$$

From the general solution of $U(x, s)$, the terms in Eq. (B.6) can be written as

$$U(0,s) = c_1 \quad \text{and} \quad \frac{\partial U}{\partial x}\Big|_{x=0} = -\sqrt{\frac{k_R + s}{D}}c_1. \tag{B.7}$$

Substituting Eqs. (B.7) into (B.6) yields coefficient c_1 as

$$c_1 = \frac{\frac{k}{\sqrt{D}}C_\infty}{s\left(\sqrt{k_R + s} + \frac{k}{\sqrt{D}}\right)}. \tag{B.8}$$

Thus, the solution for $U(x, s)$ can be written by

$$U(x,\ s) = \frac{\frac{k}{\sqrt{D}}C_\infty}{s\left(\sqrt{k_R + s} + \frac{k}{\sqrt{D}}\right)} e^{-\sqrt{\frac{k_R+s}{D}}x}. \tag{B.9}$$

Applying the shifting theorem yields

$$U(x,\ s-k_R)=\frac{\frac{k}{\sqrt{D}}C_\infty}{(s-k_R)\left(\sqrt{s}+\frac{k}{\sqrt{D}}\right)}e^{-\sqrt{\frac{s}{D}}x}. \quad \text{(B.10)}$$

For the inverse Laplace transform, the following formula was adopted from [100].

$$\mathcal{L}^{-1}\left[\frac{\sqrt{a}e^{-\sqrt{\frac{s}{a}}x}}{(s-\gamma)(\sqrt{s}+\beta\sqrt{a})}\right]=\frac{1}{2}e^{\gamma t}\left\{\frac{\sqrt{a}}{\sqrt{a}\beta+\sqrt{\gamma}}e^{-x\sqrt{\frac{\gamma}{a}}}erfc\left(\frac{x}{2\sqrt{at}}-\sqrt{\gamma t}\right)+\right. \quad \text{(B.11)}$$

$$\left.\frac{\sqrt{a}}{\sqrt{a}\beta-\sqrt{\gamma}}e^{x\sqrt{\frac{\gamma}{a}}}erfc\left(\frac{x}{2\sqrt{at}}+\sqrt{\gamma t}\right)\right\}-\frac{a\beta}{a\beta^2-\gamma}e^{\beta x+a\beta^2 t}\,erfc\left(\frac{x}{2\sqrt{at}}+\beta\sqrt{at}\right).$$

Similarly, the inverse Laplace transform in Eq. (B.10) yields

$$\begin{aligned}\mathcal{L}^{-1}\{U(x,\ s-k_R)\}&=e^{k_Rt}C(x,\ t)\\&=\frac{kC_\infty}{D}\left[\frac{1}{2}e^{k_Rt}\left\{\frac{\sqrt{D}}{\frac{k}{\sqrt{D}}+\sqrt{k_R}}e^{-x\sqrt{\frac{k_R}{D}}}erfc\left(\frac{x}{2\sqrt{Dt}}-\sqrt{k_Rt}\right)\right.\right.\\&\quad\left.+\frac{\sqrt{D}}{\frac{k}{\sqrt{D}}-\sqrt{k_R}}e^{x\sqrt{\frac{k_R}{D}}}erfc\left(\frac{x}{2\sqrt{Dt}}+\sqrt{k_Rt}\right)\right\} \quad \text{(B.12)}\\&\quad\left.-\frac{k}{\frac{k^2}{D}-k_R}e^{\left(\frac{k}{D}x+\frac{k^2}{D}t\right)}erfc\left(\frac{x}{2\sqrt{Dt}}+\frac{k\sqrt{t}}{\sqrt{D}}\right)\right].\end{aligned}$$

Finally, the solution of the C(x, t) has the form

$$\begin{aligned}\frac{C(x,\ t)}{C_\infty}&=\frac{ke^{-k_Rt}}{D}\left[\frac{1}{2}e^{k_Rt}\left\{\frac{\sqrt{D}}{\frac{k}{\sqrt{D}}+\sqrt{k_R}}e^{-x\sqrt{\frac{k_R}{D}}}erfc\left(\frac{x}{2\sqrt{Dt}}-\sqrt{k_Rt}\right)\right.\right.\\&\quad\left.+\frac{\sqrt{D}}{\frac{k}{\sqrt{D}}-\sqrt{k_R}}e^{x\sqrt{\frac{k_R}{D}}}erfc\left(\frac{x}{2\sqrt{Dt}}+\sqrt{k_Rt}\right)\right\} \quad \text{(B.13)}\\&\quad\left.-\frac{k}{\frac{k^2}{D}-k_R}e^{\left(\frac{k}{D}x+\frac{k^2}{D}t\right)}erfc\left(\frac{x}{2\sqrt{Dt}}+\frac{k\sqrt{t}}{\sqrt{D}}\right)\right].\end{aligned}$$

References

[1] H.M. H Nishimura, Plastic Deformation Behaviour Plastic Pipes Under Displacement in: 10th Plastic Pipes Conference, Gothenburg, 1998.

[2] T.H. Hideki Omuro, Polyethylene Pipeline Performance Against Earthquake in: 19th Plastic Pipes Conference, Las Vegas, 2018.

[3] J.P. Dear, N.S. Mason, Effect of chlorine on polyethylene pipes in water distribution networks, Proceedings of the Institution of Mechanical Engineers, Part L: Journal of Materials: Design and Applications, 220 (2006) 97-111.

[4] H. Zhang, L. Zhao, D. Liu, J. Wang, X. Zhang, C. Chen, Early period corrosion and scaling characteristics of ductile iron pipe for ground water supply with sodium hypochlorite disinfection, Water Research, 176 (2020) 115742.

[5] P.J. DesLauriers, M.P. McDaniel, D.C. Rohlfing, R.K. Krishnaswamy, S.J. Secora, E.A. Benham, P.L. Maeger, A.R. Wolfe, A.M. Sukhadia, B.B. Beaulieu, A comparative study of multimodal vs. bimodal polyethylene pipe resins for PE-100 applications, Polymer Engineering & Science, 45 (2005) 1203-1213.

[6] P.J. DesLauriers, D.C. Rohlfing, E.T. Hsieh, Quantifying short chain branching microstructures in ethylene 1-olefin copolymers using size exclusion chromatography and Fourier transform infrared spectroscopy (SEC–FTIR), Polymer, 43 (2002) 159-170.

[7] P.J. DesLauriers, D.C. Rohlfing, Estimating Slow Crack Growth Performance of Polyethylene Resins from Primary Structures such as Molecular Weight and Short Chain Branching, Macromolecular Symposia, 282 (2009) 136-149.

[8] R.K. Krishnaswamy, Q. Yang, L. Fernandez-Ballester, J.A. Kornfield, Effect of the Distribution of Short-Chain Branches on Crystallization Kinetics and Mechanical Properties of High-Density Polyethylene, Macromolecules, 41 (2008) 1693-1704.

[9] A.D. Channell, E.Q. Clutton, The effects of short chain branching and molecular weight on the impact fracture toughness of polyethylene, Polymer, 33 (1992) 4108-4112.

[10] X. He, X. Zha, X. Zhu, X. Qi, B. Liu, Effect of short chain branches distribution on fracture behavior of polyethylene pipe resins, Polymer Testing, 68 (2018) 219-228.

[11] Z. Tian, K.-R. Chen, B.-P. Liu, N. Luo, W.-L. Du, F. Qian, Short-chain branching distribution oriented model development for Borstar bimodal polyethylene process and its correlation with product performance of slow crack growth, Chemical Engineering Science, 130 (2015) 41-55.

[12] L. Kurelec, M. Teeuwen, H. Schoffeleers, R. Deblieck, Strain hardening modulus as a measure of environmental stress crack resistance of high density polyethylene, Polymer, 46 (2005) 6369-6379.

[13] S. Deveci, D. Fang, Correlation of molecular parameters, strain hardening modulus and cyclic fatigue test performances of polyethylene materials for pressure pipe applications, Polymer Testing, 62 (2017) 246-253.

[14] S. Deveci, S.K. Kaliappan, J. Fawaz, U. Gadgoli, B. Das, Sensitivity of post yield axial deformation properties of high-density ethylene/α-olefin copolymers in relation to molecular structure and slow crack growth resistance, Polymer Testing, 72 (2018) 285-297.

[15] J. Fawaz, S. Deveci, V. Mittal, Molecular and morphological studies to understand slow crack growth (SCG) of polyethylene, Colloid and Polymer Science, 294 (2016) 1269-1280.

[16] J. Zheng, Y. Zhang, D. Hou, Y. Qin, W. Guo, C. Zhang, J. Shi, A review of nondestructive examination technology for polyethylene pipe in nuclear power plant, Frontiers of Mechanical Engineering, 13 (2018) 535-545.

[17] Y. Qin, J. Shi, J. Zheng, D. Hou, W. Guo, An Improved Phased Array Ultrasonic Testing Technique for Thick-Wall Polyethylene Pipe Used in Nuclear Power Plant, Journal of Pressure Vessel Technology, 141 (2019) 041403.

[18] J. Shi, A. Hu, F. Yu, Y. Cui, R. Yang, J. Zheng, Finite element analysis of high-density polyethylene pipe in pipe gallery of nuclear power plants, Nuclear Engineering and Technology, 53 (2021) 1004-1012.

[19] P.A. Lee, S. Kim, B. Stakenborghs, Y. Suh, S. Choi, Development of hydro-axial tension method for whole pipe butt-fusion joint tensile test, Polymer Testing, 109 (2022) 107553.

[20] R.C. Shane Schuessler, Mohamed Hageb, Abdullah Saber, Grigorios Vigellis, Chandra Basavaraju, High Density Polytheylene (HDPE) Pipe Brings Safe Shores and Reliable Electricity to Rwanda in: 21st Plastic Pipes Conference, Orlando, 2023.

[21] S.R.S. Ali Al Hammadi, Mohamed Ali Awadh Jaber, High Density Polyethylene (HDPE): An Overview of The First Ever ASME BPVC Section III, Class 3 Nuclear Piping Installation, in: 19th Plastic Pipes Conference, Las Vegas, 2018.

[22] S.D. Mohana Murali Adhyatmabhattar, PE Pipes In Oil and Gas Industry In The Middle East, in: 16th Plastic Pipes Conference, Barcelona, 2012.

[23] J.-W. Wee, B.-H. Choi, Modeling of axisymmetric slow crack growth of high-density polyethylene with circular notched bar specimen using crack layer theory, International Journal of Solids and Structures, 97-98 (2016) 189-199.

[24] A. Chudnovsky, Z. Zhou, H. Zhang, K. Sehanobish, Lifetime assessment of engineering thermoplastics, International Journal of Engineering Science, 59 (2012) 108-139.

[25] P. Hutař, M. Ševčík, L. Náhlík, G. Pinter, A. Frank, I. Mitev, A numerical methodology for lifetime estimation of HDPE pressure pipes, Engineering Fracture Mechanics, 78 (2011) 3049-3058.

[26] A. Chudnovsky, Slow crack growth, its modeling and crack-layer approach: A review, International Journal of Engineering Science, 83 (2014) 6-41.

[27] C.J.G. Plummer, A. Goldberg, A. Ghanem, Micromechanisms of slow crack growth in polyethylene under constant tensile loading, Polymer, 42 (2001) 9551-9564.

[28] R. Schouwenaars, V.H. Jacobo, E. Ramos, A. Ortiz, Slow crack growth and failure induced by manufacturing defects in HDPE-tubes, Engineering Failure Analysis, 14 (2007) 1124-1134.

[29] ISO 4427-2:2019 Plastics piping systems for water supply, and for drainage and sewerage under pressure, Polyethylene (PE) Part 2: Pipes,

[30] ISO 4427-1:2019 Plastics piping systems for water supply and for drainage and sewerage under pressure Polyethylene (PE) Part 1: General,

[31] The Plastics Industry Pipe Association of Australia (PIPA) POP018: Polyethylene Drinking Water Pipes in Contact with Chlorine and Chloramine Disinfectants, 2019.

[32] B.-H. Choi, Z. Zhou, A. Chudnovsky, S.S. Stivala, K. Sehanobish, C.P. Bosnyak, Fracture initiation associated with chemical degradation: observation and modeling, International Journal of Solids and Structures, 42 (2005) 681-695.

[33] B.-H. Choi, A. Chudnovsky, K. Sehanobish, Stress Corrosion Cracking in Plastic Pipes: Observation and Modeling, International Journal of Fracture, 145 (2007) 81-88.

[34] B.-H. Choi, A. Chudnovsky, R. Paradkar, W. Michie, Z. Zhou, P.-M. Cham, Experimental and theoretical investigation of stress corrosion crack (SCC) growth of polyethylene pipes, Polymer Degradation and Stability, 94 (2009) 859-867.

[35] X. Colin, L. Audouin, J. Verdu, M. Rozental-Evesque, B. Rabaud, F. Martin, F. Bourgine, Aging of polyethylene pipes transporting drinking water disinfected by chlorine dioxide. I. Chemical aspects, Polymer Engineering & Science, 49 (2009) 1429-1437.

[36] A.J. Whelton, A.M. Dietrich, Critical considerations for the accelerated ageing of high-density polyethylene potable water materials, Polymer Degradation and Stability, 94 (2009) 1163-1175.

[37] W. Yu, B. Azhdar, D. Andersson, T. Reitberger, J. Hassinen, T. Hjertberg, U.W. Gedde, Deterioration of polyethylene pipes exposed to water containing chlorine dioxide, Polymer Degradation and Stability, 96 (2011) 790-797.

[38] C. Devilliers, B. Fayolle, L. Laiarinandrasana, S. Oberti, E. Gaudichet-Maurin, Kinetics of chlorine-induced polyethylene degradation in water pipes, Polymer Degradation and Stability, 96 (2011) 1361-1368.

[39] Z. Zhu, S. Xu, Y. Pei, L. Shan, W. Zheng, X. Bao, Y. Yuan, Assessment of the microbiological safety of drinking water in outdoor pipe materials: biofilm formation and chlorine resistance of typical bacteria, Environmental Science: Water Research & Technology, (2023).

[40] X. Zhang, T. Lin, F. Jiang, X. Zhang, S. Wang, S. Zhang, Impact of pipe material and chlorination on the biofilm structure and microbial communities, Chemosphere, 289 (2022) 133218.

[41] X. Yan, T. Lin, X. Wang, S. Zhang, K. Zhou, Effects of pipe materials on the characteristic recognition, disinfection byproduct formation, and toxicity risk of pipe wall biofilms during chlorination in water supply pipelines, Water Research, 210 (2022) 117980.

[42] S.M. Mitroka, T.D. Smiley, J.M. Tanko, A.M. Dietrich, Reaction mechanism for oxidation and degradation of high density polyethylene in chlorinated water, Polymer Degradation and Stability, 98 (2013) 1369-1377.

[43] J. Castillo Montes, D. Cadoux, J. Creus, S. Touzain, E. Gaudichet-Maurin, O. Correc, Ageing of polyethylene at raised temperature in contact with chlorinated sanitary hot water. Part I – Chemical aspects, Polymer Degradation and Stability, 97 (2012) 149-157.

[44] ASTM F2263, Standard Test Method for Evaluating the Oxidative Resistance of Polyethylene (PE) Pipe to Chlorinated Water, West Conshohocken, PA, 2014.

[45] ASTM F2023, Standard Test Method for Evaluating the Oxidative Resistance of Crosslinked Polyethylene (PEX) Pipe, Tubing and Systems to Hot Chlorinated Water, West Conshohocken, PA, 2021.

[46] ASTM F3497, Standard Test Method for Evaluating the Oxidative Resistance of Polypropylene (PP) Piping Systems to Hot Chlorinated Water, West Conshohocken, PA, 2021.

[47] XP T 54-986, “Polyolefin pipes for the conveyance of fluids under pressure – Determination of circumferential tensile properties of a pipe”, 2013.

[48] K. Majewski, S.C. Mantell, M. Bhattacharya, Relationship between morphological changes and mechanical properties in HDPE films exposed to a chlorinated environment, Polymer Degradation and Stability, 171 (2020) 109027.

[49] A. Mikdam, X. Colin, G. Minard, N. Billon, R. Maurin, A kinetic model for predicting the oxidative degradation of additive free polyethylene in bleach desinfected water, Polymer Degradation and Stability, 146 (2017) 78-94.

[50] M. Bredács, A. Frank, A. Bastero, A. Stolarz, G. Pinter, Accelerated aging of polyethylene pipe grades in aqueous chlorine dioxide at constant concentration, Polymer Degradation and Stability, 157 (2018) 80-89.

[51] W. Yu, E. Sedghi, S. Nawaz, T. Hjertberg, J. Oderkerk, F.R. Costa, U.W. Gedde, Assessing the long-term performance of polyethylene stabilised with phenolic antioxidants exposed to water containing chlorine dioxide, Polymer Testing, 32 (2013) 359-365.

[52] X.-F. Wei, K.J. Kallio, S. Bruder, M. Bellander, H.-H. Kausch, U.W. Gedde, M.S. Hedenqvist, Diffusion-limited oxidation of polyamide: Three stages of fracture behavior, Polymer Degradation and Stability, 154 (2018) 73-83.

[53] A. Quintana, M.C. Celina, Overview of DLO modeling and approaches to predict heterogeneous oxidative polymer degradation, Polymer Degradation and Stability, 149 (2018) 173-191.

[54] K.T. Gillen, R.L. Clough, Rigorous experimental confirmation of a theoretical model for diffusion-limited oxidation, Polymer, 33 (1992) 4358-4365.

[55] L. Audouin, V. Langlois, J. Verdu, J.C.M. De Bruijn, Role of oxygen diffusion in polymer ageing: kinetic and mechanical aspects, Journal of Materials science, 29 (1994) 569-583.

[56] S. Zha, H.-q. Lan, N. Lin, T. Meng, Degradation and characterization methods for polyethylene gas pipes after natural and accelerated aging, Polymer Degradation and Stability, 208 (2023) 110247.

[57] M. Celina, K.T. Gillen, R.A. Assink, Accelerated aging and lifetime prediction: Review of non-Arrhenius behaviour due to two competing processes, Polymer Degradation and Stability, 90 (2005) 395-404.

[58] ISO 18489:2015 Polyethylene (PE) materials for piping systems, Determination of resistance to slow crack growth under cyclic loading, Cracked Round Bar test method,

[59] J. Fischer, P.J. Freudenthaler, P.R. Bradler, R.W. Lang, Novel test system and test procedure for fatigue crack growth testing with cracked round bar (CRB) specimens, Polymer Testing, 78 (2019) 105998.

[60] J. Fischer, P.R. Bradler, R.W. Lang, Test equipment for fatigue crack growth testing of polymeric materials in chlorinated water at different temperatures, Engineering Fracture Mechanics, 203 (2018) 44-53.

[61] A. Frank, F.J. Arbeiter, I.J. Berger, P. Hutař, L. Náhlík, G. Pinter, Fracture Mechanics Lifetime Prediction of Polyethylene Pipes, Journal of Pipeline Systems Engineering and Practice, 10 (2019) 04018030.

[62] G. Pinter, M. Haager, W. Balika, R.W. Lang, Fatigue crack growth in PE-HD pipe grades, Plastics, Rubber and Composites, 34 (2005) 25-33.

[63] G. Pinter, M. Haager, W. Balika, R.W. Lang, Cyclic crack growth tests with CRB specimens for the evaluation of the long-term performance of PE pipe grades, Polymer Testing, 26 (2007) 180-188.

[64] Y. Zhao, B.-H. Choi, A. Chudnovsky, Characterization of the fatigue crack behavior of pipe grade polyethylene using circular notched specimens, International Journal of Fatigue, 51 (2013) 26-35.

[65] I. Kim, Y. Zhao, B.-H. Choi, J.M. Lee, K.-S. Lee, J.-M. Lee, Numerical analysis of asymmetric fatigue crack growth behaviors of circular notched bar specimen resulting from various geometric misalignments, Engineering Fracture Mechanics, 108 (2013) 50-64.

[66] J.-W. Wee, A. Chudnovsky, B.-H. Choi, Modeling of multiple crack initiation in polymer pipes under oxidative environment, International Journal of Engineering Science, 176 (2022) 103686.

[67] P. Vibien, J. Couch, K. Oliphant, W. Zhou, B. Zhang, A. Chudnovsky, Assessing material performance in chlorinated potable water applications, 11th Plastic Pipes, Munich, Germany, (2001) 863-872.

[68] M. Parsons, E.V. Stepanov, A. Hiltner, E. Baer, Effect of strain rate on stepwise fatigue

and creep slow crack growth in high density polyethylene, Journal of Materials Science, 35 (2000) 1857-1866.

[69] M. Parsons, E.V. Stepanov, A. Hiltner, E. Baer, The damage zone ahead of the arrested crack in polyethylene resins, Journal of Materials Science, 36 (2001) 5747-5755.

[70] M. Parsons, E.V. Stepanov, A. Hiltner, E. Baer, Correlation of stepwise fatigue and creep slow crack growth in high density polyethylene, Journal of Materials Science, 34 (1999) 3315-3326.

[71] W. Balika, G. Pinter, R.W. Lang, Systematic investigations of fatigue crack growth behavior of a PE-HD pipe grade in through-thickness direction, Journal of Applied Polymer Science, 103 (2007) 1745-1758.

[72] A. Frank, K. Bruckmoser, A. Redhead, D.P. Gruber, G. Pinter, Investigation of the Slow Crack Growth Behavior of Static and Cyclic Loaded Specimens of Polyethylene by 2D and 3D Optical Fracture Surface Analysis, Macromolecular Symposia, 311 (2012) 103-111.

[73] A. Shah, E.V. Stepanov, G. Capaccio, A. Hiltner, E. Baer, Stepwise fatigue crack propagation in polyethylene resins of different molecular structure, Journal of Polymer Science Part B: Polymer Physics, 36 (1998) 2355-2369.

[74] A. Chudnovsky, Z. Zhou, H. Zhang, K. Sehanobish, Ductile-Brittle Transition in Mechanisms of Slow Crack Growth in Engineering Thermoplastics, Procedia Engineering, 10 (2011) 1473-1478.

[75] A. Chudnovsky, A. Moet, Thermodynamics of translational crack layer propagation, Journal of Materials Science, 20 (1985) 630-635.

[76] H. Zhang, Z. Zhou, A. Chudnovsky, Applying the crack-layer concept to modeling of slow crack growth in polyethylene, International Journal of Engineering Science, 83 (2014) 42-56.

[77] J.-W. Wee, B.-H. Choi, Prediction of discontinuous fatigue crack growth in high density polyethylene based on the crack layer theory with variable crack layer parameters, International Journal of Fatigue, 92 (2016) 304-312.

[78] B.-H. Choi, W. Balika, A. Chudnovsky, G. Pinter, R.W. Lang, The use of crack layer theory to predict the lifetime of the fatigue crack growth of high density polyethylene, Polymer Engineering & Science, 49 (2009) 1421-1428.

[79] J.-W. Wee, I. Kim, M.-S. Choi, S.-K. Park, B.-H. Choi, Characterization and modeling of slow crack growth behaviors of defective high-density polyethylene pipes using stiff-constant K specimen, Polymer Testing, 86 (2020) 106499.

[80] J.-W. Wee, S.-Y. Park, B.-H. Choi, Modeling and application of discontinuous slow crack growth behaviors of high-density polyethylene pipe with various geometries and loading conditions, Engineering Fracture Mechanics, 236 (2020) 107205.

[81] K. Kadota, A. Chudnovsky, Constitutive equations of crack layer growth, Polymer Engineering & Science, 32 (1992) 1097-1104.

[82] D. Castagnetti, G. Scirè Mammano, E. Dragoni, Effect of chlorinated water on the oxidative resistance and the mechanical strength of polyethylene pipes, Polymer Testing, 30 (2011) 277-285.

[83] I.A. Khan, K.H. Lee, Y.-S. Lee, J.-O. Kim, Degradation analysis of polymeric pipe materials used for water supply systems under various disinfectant conditions, Chemosphere, 291 (2022) 132669.

[84] G. Mittelman, J.H. Davidson, S.C. Mantell, Y. Su, Prediction of polymer tube life for solar hot water systems: A model of antioxidant loss, Solar Energy, 82 (2008) 452-461.

[85] D.E. Duvall, D.B. Edwards, Forensic Analysis of Oxidation Embrittlement in Failed HDPE Potable Water Pipes, in: Pipelines 2010: Climbing New Peaks to Infrastructure Reliability: Renew, Rehab, and Reinvest, 2010, pp. 648-662.

[86] D.E. Duvall, D.B. Edwards, Field Failure Mechanisms in HDPE Potable-Water Pipe, Plastics Engineering, 68 (2012) 12-19.

[87] S. Tantry, D. Anantharaman, B.H.S. Thimmappa, R. Kamalakaran, Studying banded spherulites in HDPE by electron microscopy, Polymer Testing, 89 (2020) 106631.

[88] A. Redhead, A. Frank, G. Pinter, Investigation of slow crack growth initiation in polyethylene pipe grades with accelerated cyclic tests, Engineering Fracture Mechanics, 101 (2013) 2-9.

[89] J.-W. Wee, B.-H. Choi, Modeling of stress corrosion crack growth and lifetime of pipe grade high density polyethylene by using crack layer theory, Transactions of the Korean Society of Pressure Vessels and Piping, 11 (2015) 45-50.

[90] J.-W. Wee, I. Kim, B.-H. Choi, Development of mechanochemical degradation induced slow crack growth model for high density polyethylene in cracked round bar specimen, Journal of Mechanical Science and Technology, 37 (2023) 719-726.

[91] X.R. Wu, J. Carlsson, Weight Functions and Stress Intensity Factor Solutions, Pergamon Press, 1991.

[92] P.C. Paris, G.C. Sih, Stress analysis of cracks, ASTM stp, 381 (1965) 30-81.

[93] H. Tada, P.C. Paris, G.R. Irwin, The Stress Analysis of Cracks Handbook, Third Edition, ASME Press 2000.

[94] B.-H. Choi, A. Chudnovsky, Stress Corrosion Crack Growth in Pipe Grade Steels in Near Neutral pH Environment, International Journal of Fracture, 116 (2002) 43-48.

[95] J. Viebke, U.W. Gedde, Antioxidant diffusion in polyethylene hot-water pipes, Polymer Engineering & Science, 37 (1997) 896-911.

[96] J.-W. Wee, B.-H. Choi, Impact of material and physical parameters of the crack layer theory on slow crack growth behavior of high density polyethylene, Engineering Fracture Mechanics, 175 (2017) 101-114.

[97] R.W. Lang, A. Stern, G. Doerner, Applicability and limitations of current lifetime prediction models for thermoplastics pipes under internal pressure, Die Angewandte Makromolekulare Chemie, 247 (1997) 131-145.

[98] A. Chudnovsky, Y. Shulkin, Application of the crack layer theory to modeling of slow crack growth in polyethylene, International Journal of Fracture, 97 (1999) 83-102.

[99] L. Onsager, Reciprocal Relations in Irreversible Processes. I, Physical Review, 37 (1931) 405-426.

[100] V.S. Arpaci, Conduction Heat Transfer, Addison-Wesley, 1966.

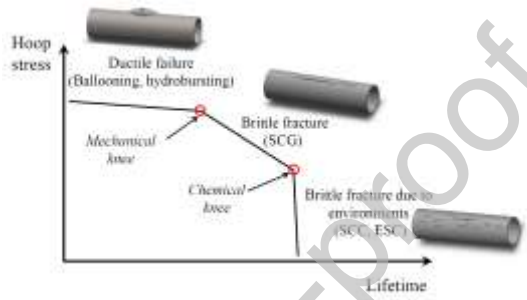

Fig. 1. Different failure behaviors of polyethylene pipe with an applied hoop stress [23].

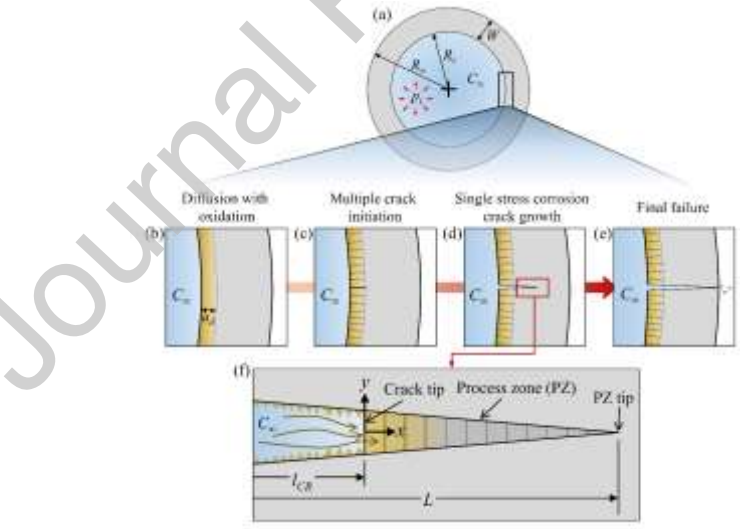

Fig. 2. Failure stages of the pressurized polyethylene pipe conveying oxidative agents depicted in (a): (b) Diffusion of the oxidative agent into the inner surface with the formation of thin degradation layer, (c) formation of multiple initial cracks, (d) slow crack growth (SCG) of a main crack, and (e) final failure. The enlarged view of the crack layer (CL) system in the SCG stage is shown in (f).

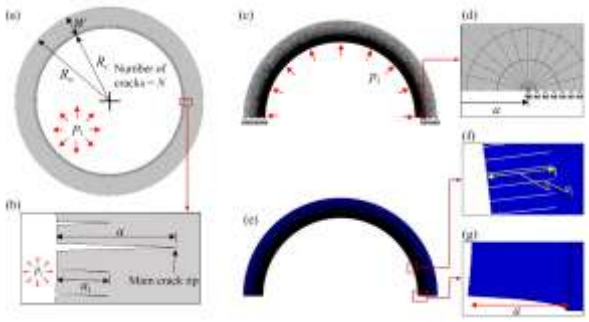

Fig. 3. (a) Configuration of the main crack after multiple crack initiation (N cracks) under internal pressure p_i. The enlarged view of the main crack is shown in (b), where the main crack and multiple crack initiation lengths are denoted by a and a_i, respectively. (c) The FEA model determines the stress intensity factor (SIF) of the main crack tip, and the crack tip model for singularity is shown in (d). The deformation caused by p_i is shown in (e), with the enlarged views (f) and (g).

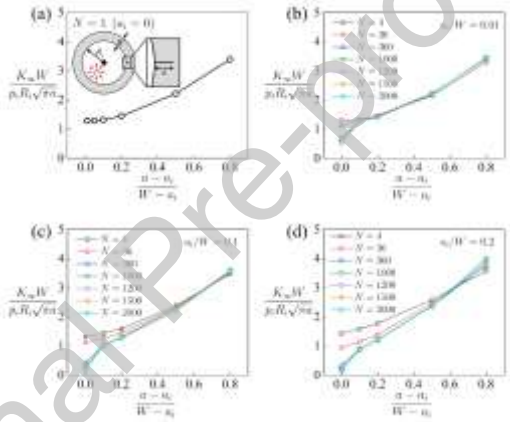

Fig. 4. Normalized SIF (K_∞) of the main crack tip caused by the internal pressure (p_i). (a) Single crack initiation case (a_i = 0) with various crack lengths (a). (b) Normalized K_∞ with various crack initiation numbers (N), when the normalized crack initiation lengths (a_i/W) of 0.01. The normalized K_∞ for a_i/W = 0.1 and 0.2 are shown in (c) and (d), respectively.

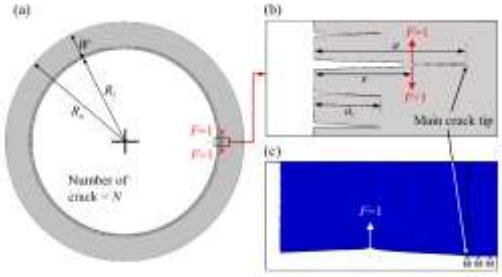

Fig.5. (a) Multiple cracks with a single main crack under the unit dipole force $F = 1$ on x. Enlarged view near the main crack is shown in (b). (c) Deformation caused by the unit dipole force.

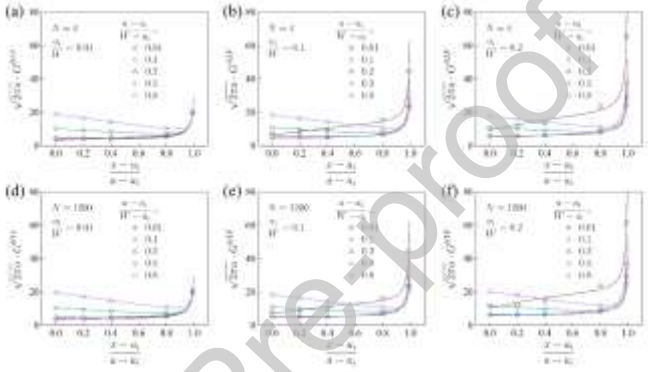

Fig. 6. SIF Green's function (G^{SIF}) with a unit dipole force at location x. Here, x is normalized by the initial crack length (a_i) and main crack length (a), i.e., $(x\text{-}a_i)/(a\text{-}a_i)$. At the number of initial cracks (N) of 4, the G^{SIF} of various $(a\text{-}a_i)/(W\text{-}a_i)$ with normalized x for a_i/W = 0.01, 0.1, and 0.2 are shown in (a), (b), and (c), respectively, where W indicates the pipe wall thickness. Same plots for N = 1200 are shown in (d), (e), and (f), respectively.

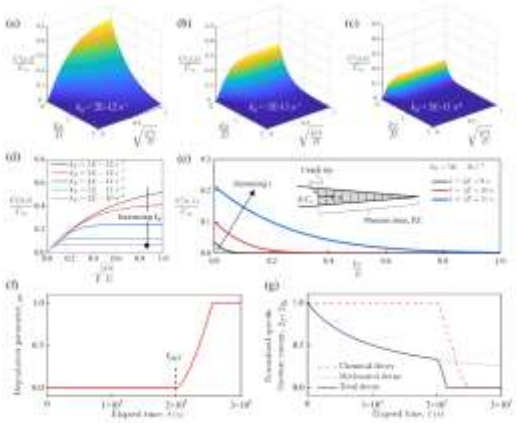

Fig. 7. Diffusion behavior of an oxidative agent with a chemical reaction. The normalized concentration of the PZ medium, $C(x, t)/C_\infty$ for reaction rate constants (k_R) of 2E-12, 1E-11, and 5E-11 s^{-1} are shown in (a), (b), and (c), respectively. The increase in the

concentration on the crack tip (x = 0) is shown in (d) for various k_R. The concentration profiles along the PZ medium at different elapsed times are shown in (e). (f) Degradation parameter ω with the elapsed time considering the oxidation induction time t_{OIT}. (g) The decrease of specific fracture energy with elapsed time. The mechanical and chemical decay are denoted by blue and red dotted curves, and the total decay is given by the superposition, represented by the black solid curve.

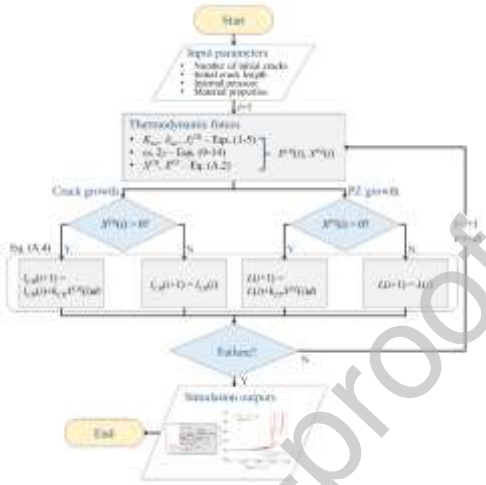

Fig. 8. Algorithms for crack layer growth simulation after the multiple crack initiation in oxidative environment.

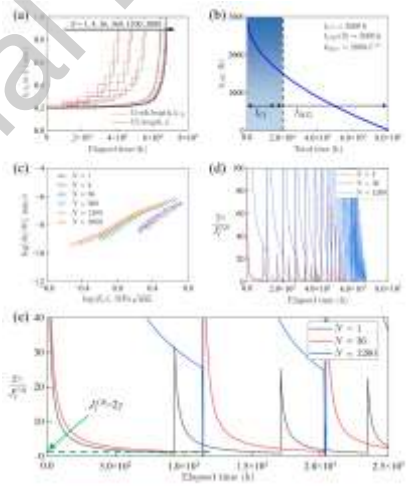

Fig. 9. Effect of the number of initial cracks (N) on the SCG behavior. The discontinuous CL growth for N = 1, 4, 36, 360, 1200, and 2000 are shown in (a), where the crack length (l_{CR}) and CL length (L) are represented by black and red curves, respectively. (b) The decrease in the oxidation induction time (t_{OIT}) with the total operation time of pipe. (c) The SCG rate (da/dt) against the SIF (K_I). The SFE (2γ) normalized by the energy release rate (J_I^{CR}) during the discontinuous SCG behavior with N is plotted in (d), and the enlarged view at the initial crack is shown in (e). The instance at which the crack jumps, where the $J_I^{CR} = 2\gamma$ is represented in the green dotted horizontal line in (e).

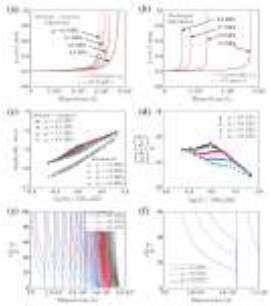

Fig. 10. Effect of internal pressure (p_i) on the SCG behavior. The discontinuous CL growth for p_i = 0.5, 0.6, 0.7, and 0.8 MPa are shown in (a), where l_{CR} and L are represented by black and red curves, respectively. For the comparison, the SCG behavior under the mechanical degradation only, i.e., without chemical degradation, is also provided in (b). The SCG rate (da/dt) against the SIF (K_I) for the mechanochemical and mechanical degradation cases are compared in (c). The ratio of the SCG rate under mechanochemical degradation $(da/dt)_{mc}$ to that under mechanical degradation $(da/dt)_m$ for different pi are plotted in (d). The SFE (2γ) normalized by the energy release rate (J_I^{CR}) during the discontinuous SCG behavior with p_i is plotted in (e), and the enlarged view at the initial crack is shown in (f).

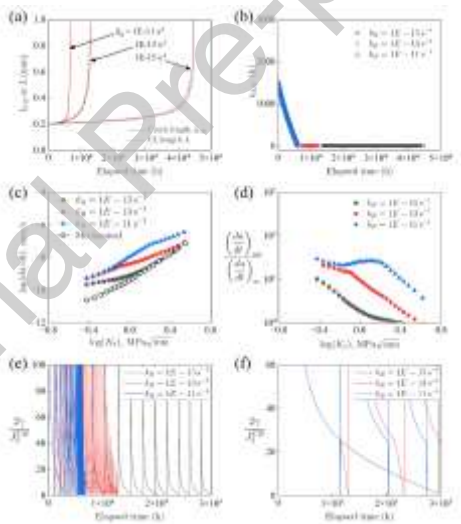

Fig. 11. Effect of the reaction rate constant (k_R) on the SCG behavior. The discontinuous CL growth for k_R =1E−11, 1E−13, and 1E−15 s^{-1} are shown in (a), where l_{CR} and L are represented by black and red curves, respectively. The decrease in oxidation induction time (t_{OIT}) with the SCG period at different k_R is shown in (b). The SCG rate (da/dt) against the SIF (K_I) for the different k_R (mechanochemical) and mechanical degradation cases are depicted in (c). The ratio of the SCG rate under mechanochemical degradation $(da/dt)_{mc}$ to that under mechanical degradation $(da/dt)_m$ for different k_R is plotted in (d). The SFE (2γ) normalized by the energy release rate (J_I^{CR}) during the discontinuous SCG behavior with k_R is plotted in (e), and the enlarged view at the initial crack is also shown in (f).

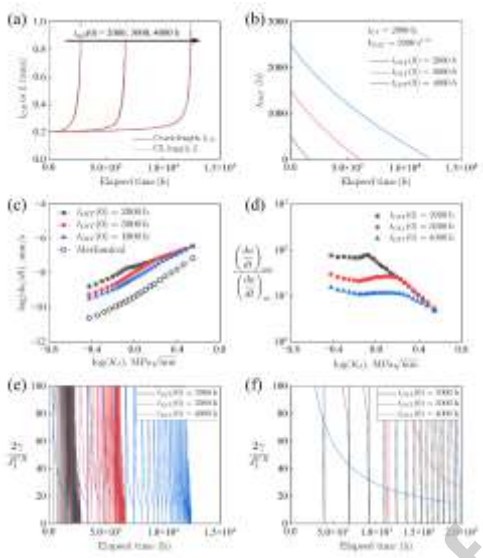

Fig. 12. Effect of the initial oxidation induction time $t_{OIT}(0)$ on the SCG behavior. The discontinuous CL growth for $t_{OIT}(0)$ =2000, 3000, and 4000 h are shown in (a), where l_{CR} and L are represented by black and red curves, respectively. The decrease in t_{OIT} with the SCG period at different $t_{OIT}(0)$ values is shown in (b). The SCG rate (da/dt) against the SIF (K_I) for the different k_R (mechanochemical) and mechanical degradation cases are depicted in (c). The ratio of the SCG rate under mechanochemical degradation $(da/dt)_{mc}$ to that under the mechanical degradation $(da/dt)_m$ for different $t_{OIT}(0)$ is plotted in (d). The SFE (2γ) normalized by the energy release rate (J_I^{CR}) during the discontinuous SCG behavior with $t_{OIT}(0)$ is plotted in (e); the enlarged view at the initial crack is also shown in (f).

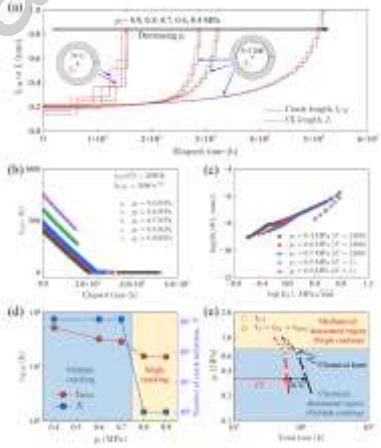

Fig. 13. (a) SCG behavior under different internal pressures (p_i), where the initial crack length (a_i), number of initial cracks (N), and crack initiation time (t_{CI}) with p_i are listed in Table 7. Under the p_i of 0.9 and 0.8 MPa, the SCG simulations were conducted from single crack initiation (N = 1), whereas N = 1200 was considered for p_i = 0.7, 0.6, and 0.4 MPa. (b) Decrease in the oxidation induction time (t_{OIT}) with the SCG period under different p_i. (c) SCG rate (da/dt) against the SIF (K_I) for different p_i. (d) SCG duration (t_{SCG}) and N with p_i. (e) Estimated p_i - total lifetime (t_f) plot based on the proposed model, where both t_{CI} and t_{SCG} were considered and the chemical knee points dividing the

mechanical- (single cracking) and chemical-dominated regions (multiple cracking) were observed.

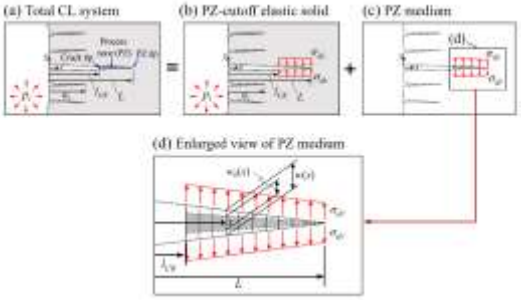

Fig. A.1. The CL system of the main crack after the multiple crack initiation (N cracks) of a pressurized pipe: (a) Total CL system with the crack length of l_{CR} and the CL length of L. (b) Process zone (PZ)-cut-off elastic medium, (c) PZ medium, and (d) enlarged view of PZ medium. σ_{dr} denotes the hypothetical traction along the PZ boundary, which is the same with the drawing stress of the polyethylene material.

Table 1. Normalized stress intensity factor (SIF) caused by the internal pressure, $K_\infty W/(p_i R_i (\pi a)^{0.5})$, for a single inner crack (N = 1) under internal pressure p_i.

a/W	$K_\infty W/(p_i R_i (\pi a)^{0.5})$
0.01	1.280
0.05	1.287
0.1	1.310
0.2	1.446
0.5	2.211
0.8	3.391

Table 2. Normalized SIF attributed to the internal pressure $K_\infty W/(p_i R_i (\pi a)^{0.5})$ for multiple initial cracks under internal pressure p_i.

$\frac{a-a_i}{W-a_i}$	$\frac{a_i}{W}$	N						
		4	36	360	1000	1200	1500	2000
0	0.01	1.300	1.297	1.103	0.7151	0.6604	0.5969	0.5262
	0.05	1.297	1.240	0.5500	0.3408	0.3182	0.2926	0.2520
	0.1	1.319	1.128	0.4121	0.2647	0.2393	0.2156	0.1911
	0.2	1.428	0.9362	0.3266	0.2081	0.1934	0.1703	0.1567
0.01	0.01	1.258	1.255	1.108	0.9905	0.9827	0.9584	0.9558
	0.05	1.207	1.154	0.6339	0.5508	0.5448	0.5448	0.5388
	0.1	1.282	1.098	0.5090	0.4424	0.4339	0.4288	0.4214
	0.2	1.413	0.9191	0.3974	0.3428	0.3350	0.3275	0.3227
0.1	0.01	1.337	1.326	1.307	1.294	1.290	1.276	1.273
	0.05	1.371	1.321	1.159	1.139	1.136	1.134	1.132
	0.1	1.430	1.260	1.034	1.015	1.014	1.012	1.010
	0.2	1.580	1.139	0.8942	0.8785	0.8764	0.8741	0.8856

0.2	0.01	1.458	1.463	1.440	1.430	1.426	1.412	1.402
	0.05	1.518	1.475	1.378	1.363	1.362	1.360	1.358
	0.1	1.596	1.451	1.306	1.290	1.291	1.289	1.278
	0.2	1.774	1.387	1.216	1.205	1.203	1.200	1.211
0.5	0.01	2.152	2.229	2.222	2.217	2.214	2.210	2.207
	0.05	2.294	2.281	2.252	2.227	2.240	2.240	2.242
	0.1	2.378	2.322	2.289	2.276	2.278	2.273	2.205
	0.2	2.583	2.454	2.373	2.370	2.356	2.364	2.357
0.8	0.01	3.310	3.416	3.445	3.451	3.444	3.452	3.452
	0.05	3.428	3.326	3.363	3.442	3.515	3.383	3.518
	0.1	3.466	3.531	3.586	3.586	3.501	3.573	3.549
	0.2	3.582	3.745	3.854	3.767	3.981	3.991	4.003

Table 3. Coefficient c_1, c_2, and c_3 for a single crack (N = 1) in Eq. (5).

a/W	c_1	c_2	c_3
0.01	2.000	1.006	0.6204
0.05	2.000	1.130	0.5642
0.1	2.000	1.340	0.5773
0.2	2.000	2.268	0.5908
0.5	2.000	6.416	2.231
0.8	2.000	13.21	4.317

Table 4. Coefficient c_1 for the multiple initial cracks of Eq. (5).

$\frac{a-a_i}{W-a_i}$	$\frac{a_i}{W}$	N						
		4	36	360	1000	1200	1500	2000
0.01	0.01	1.920	1.920	1.927	1.921	1.920	1.920	1.920
	0.05	4.059	4.059	4.067	4.058	4.057	3.390	3.390
	0.1	4.341	4.340	4.351	4.339	4.338	4.338	4.338
	0.2	6.425	5.409	5.428	6.422	5.981	5.650	5.870
0.1	0.01	2.049	2.075	2.050	2.022	2.049	1.924	1.924
	0.05	2.439	2.439	2.407	2.445	2.454	2.462	2.465
	0.1	2.825	2.825	2.831	2.862	2.854	2.863	2.879
	0.2	3.698	3.691	3.692	3.654	3.672	3.696	2.934
0.2	0.01	2.036	2.015	2.079	2.091	2.068	2.039	1.985
	0.05	2.203	2.204	2.171	2.207	2.217	2.222	2.226
	0.1	2.426	2.426	2.429	2.446	2.445	2.449	2.436
	0.2	2.943	2.943	2.945	2.916	2.929	2.945	2.810
0.5	0.01	1.936	2.010	2.022	2.019	2.018	2.017	2.005
	0.05	2.095	2.080	2.082	2.065	2.084	2.084	2.086
	0.1	2.178	2.173	2.198	2.192	2.194	2.188	2.109
	0.2	2.425	2.424	2.419	2.426	2.408	2.420	2.402
0.8	0.01	1.958	2.000	2.048	2.047	2.043	2.048	2.045
	0.05	2.046	1.945	1.945	1.996	2.049	1.947	2.064
	0.1	2.098	2.104	2.098	2.081	2.017	2.064	2.040

	0.2	2.266	2.265	2.259	2.278	2.267	2.257	2.219

Table 5. Coefficient c_2 for the multiple initial cracks of Eq. (5).

$\frac{a-a_i}{W-a_i}$	$\frac{a_i}{W}$	N						
		4	36	360	1000	1200	1500	2000
0.01	0.01	5.008	5.006	4.985	5.026	5.112	5.059	5.083
	0.05	3.366	3.365	3.330	3.686	3.783	7.501	7.632
	0.1	13.12	13.13	13.17	14.02	14.20	13.92	14.14
	0.2	18.98	23.78	23.85	19.87	22.03	23.57	23.20
0.1	0.01	1.700	1.490	1.682	1.854	1.706	2.139	2.140
	0.05	1.617	1.618	1.817	1.693	1.649	1.628	1.637
	0.1	1.953	1.959	2.036	1.987	2.058	2.042	1.997
	0.2	1.965	2.022	2.275	2.705	2.644	2.562	7.008
0.2	0.01	2.365	2.511	2.154	2.096	2.173	2.198	2.385
	0.05	2.639	2.632	2.819	2.665	2.624	2.604	2.598
	0.1	2.906	2.914	2.953	2.900	2.968	2.928	2.999
	0.2	3.128	3.155	3.304	3.621	3.585	3.535	4.282
0.5	0.01	6.294	6.514	6.441	6.455	6.436	6.424	7.378
	0.05	6.512	6.605	6.679	6.637	6.662	6.667	6.681
	0.1	6.652	6.684	6.788	6.850	6.873	6.892	6.786
	0.2	6.816	6.917	7.140	7.511	7.565	7.680	7.841
0.8	0.01	12.87	13.38	13.33	13.34	13.32	13.35	13.37
	0.05	13.24	12.95	13.03	13.28	13.52	13.13	13.46
	0.1	13.27	13.37	13.48	13.52	13.27	13.52	13.48
	0.2	13.35	13.55	13.86	14.55	14.67	14.87	15.06

Table 6. Coefficient c_3 for the multiple initial cracks of Eq. (5).

$\frac{a-a_i}{W-a_i}$	$\frac{a_i}{W}$	N						
		4	36	360	1000	1200	1500	2000
0.01	0.01	−3.491	−3.488	−3.469	−3.486	−3.572	−3.519	−3.476
	0.05	−2.492	−2.491	−2.441	−2.537	−2.543	−5.633	−5.585
	0.1	−11.01	−11.03	−10.98	−11.37	−11.43	−10.82	−10.79
	0.2	−16.06	−20.14	−20.03	−16.13	−17.64	−18.46	−18.18
0.1	0.01	0.2343	0.4026	0.2495	0.1115	0.2351	−0.1380	−0.1374
	0.05	0.1256	0.1262	−0.0175	0.1359	0.1881	0.2256	0.2475
	0.1	−0.2141	−0.2180	−0.1698	0.0454	0.0203	0.0770	0.1669
	0.2	−0.1217	−0.1582	−0.0835	−0.1506	−0.0427	0.0951	−3.593
0.2	0.01	0.5015	0.3871	0.6804	0.7313	0.6601	0.6180	0.4452
	0.05	0.2834	0.2912	0.1463	0.2842	0.3206	0.3400	0.3560
	0.1	0.1022	0.1014	0.1111	0.2261	0.1883	0.2493	0.1644
	0.2	0.0797	0.0826	0.1340	0.0809	0.1497	0.2396	−0.3218

0.5	0.01	2.074	2.156	2.215	2.205	2.217	2.217	0.4971
	0.05	2.148	2.089	2.096	2.082	2.112	2.106	2.114
	0.1	2.000	2.005	2.047	2.040	2.056	2.055	1.945
	0.2	1.821	1.861	1.895	2.077	2.081	2.131	2.165
0.8	0.01	4.076	4.126	4.301	4.311	4.313	4.326	4.319
	0.05	3.688	3.463	3.549	3.712	3.847	3.600	3.939
	0.1	3.074	3.159	3.269	3.375	3.284	3.444	3.429
	0.2	1.987	2.173	2.555	3.277	3.360	3.424	3.564

Table 7. Input parameters for the parametric study of the single crack layer growth simulation after the multiple crack initiation of polyethylene pipe.

Parameters	Symbol	Unit	Value
Outer radius of pipe	R_o	mm	6.1595
Inner radius of pipe	R_i	mm	7.9375
Number of initial cracks	N	-	1–2000
Initial crack length	a_i	mm	0.2
Crack initiation time	t_{CI}	h	2000
Internal pressure	p_i	MPa	0.6
Drawing stress	σ_{dr}	MPa	5
Plane strain elastic modulus	E	MPa	100
Initial specific fracture energy	γ_0	mJ/mm^2	15
Natural drawing ratio	λ	-	5
Transformation energy density	γ^{tr}	mJ/mm^3	5
Characteristic time for mechanical decay	t^*	s	5000
Mass transfer coefficient	k	mm/s	1E−11
Diffusion coefficient	D	mm^2/s	1E−10
Reaction rate constant	k_R	s^{-1}	1E−11
Initial oxidation induction time	$t_{OIT}(0)$	h	3000
Reduction coefficient of oxidation induction time	k_{OIT}	s$^{0.5}$	2000
Oxidant concentration in the environment	C_∞	ppm	1
Constant for degradation parameter	k_ω	ppm^{-1}	1E+7

Table 8. Simulated crack initiation periods (t_{CI}), initial crack lengths (a_i), and number of initial cracks (N) with the applied internal pressure (p_i) [66].

p_i (MPa)	t_{CI} (h)	N	a_i (mm)
0.4	6045	1200	0.2114
0.6	5800	1200	0.2016
0.7	5655	1200	0.1955
0.8	5150	1	0.1737
0.9	4520	1	0.1428

Graphical abstract

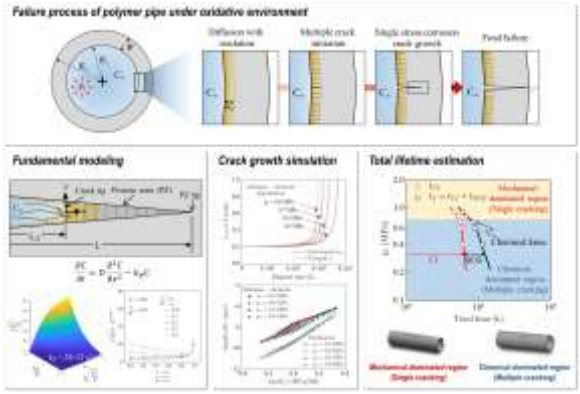

Prime Novelty Statement:

This study reveals that the process zone in front of the main crack tip of a polyethylene pipe undergoes mechanochemical deterioration, and the discontinuous SCG of the main crack leads to final failure. The study theoretically simulated the mechanochemical discontinuous SCG behavior of the main crack after multiple crack initiations on a polyethylene pipe. A new lifetime prediction methodology based on the modified crack layer theory was proposed, and successful lifetime estimation was achieved based on internal pressure, capturing the chemical knee point that classifies the failure mechanism into mechanical- (single crack initiation) and chemical-dominated regions (multiple crack initiation).

Declaration of interests

☒ The authors declare that they have no known competing financial interests or personal relationships that could have appeared to influence the work reported in this paper.

☐The authors declare the following financial interests/personal relationships which may be considered as potential competing interests: